THE JOURNAL OF PHYSICAL CHEMISTRY B

Article

pubs.acs.org/JPCB

Sodium Dodecyl Sulfate at Water–Hydrophobic Interfaces: A Simulation Study

Robert Vácha*,† and Sylvie Roke‡

†National Centre for Biomolecular Research, Faculty of Science and CEITEC—Central European Institute of Technology, Masaryk University, Kamenice 5, 625 00 Brno-Bohunice, Czech Republic

‡Laboratory for Fundamental BioPhotonics (LBP), Institute of Bioengineering (IBI), School of Engineering (STI), École Polytechnique Fédérale de Lausanne (EPFL), 1015 Lausanne, Switzerland

ABSTRACT: Using molecular dynamics simulations, we have studied the water–vapor and water–oil (decane) interfaces of aqueous solutions of sodium dodecyl sulfate (SDS). The water–vapor interface is often used as a model for water–oil (hydrophobic) interfaces, yet we observe that the behavior of amphiphilic DS^- ions at these two interfaces is very different. Specifically, on a water–vapor interface, SDS forms aggregates at low coverages, while it is homogeneously distributed on the water–oil interface. Two decane parametrizations resulted in dramatically different conformations: decane parametrized based on a GROMOS force field "froze", while decane parametrized with a TraPPE force field remained liquid at 300 K. The calculated effective second-order susceptibilities and nonlinear sum frequency scattering intensities of DS^- ions at the "frozen" decane–water agree well with experimental data of DS^- ions at the hexadecane droplet–water interface. This suggests that the orientation of longer alkane molecules is predominantly parallel to the interface and that, at low coverages, DS^- ions follow the orientation of oil molecules.

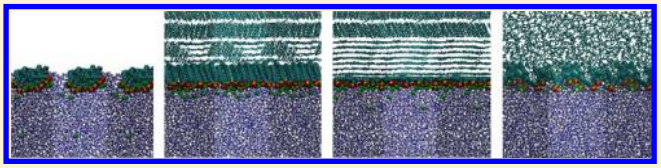

INTRODUCTION

The behavior of amphiphilic molecules at the water–vapor and water–liquid interfaces is important for many chemical processes in nature and industry. An important advance in the in situ study of interfacial structures came with the introduction of nonlinear spectroscopy.[1,2] Sum frequency generation and second harmonic generation spectroscopies are sensitive to the presence of molecules in an environment that lacks inversion symmetry. Both techniques are therefore well suited to the study of structure, orientation, and order at liquid interfaces.[3−9] Whereas these spectroscopic techniques have been used extensively to study the structure of the water–vapor interface,[9−11] the study of the interface of water in contact with another liquid (e.g., oil) has proven to be challenging.[12−14] Sum frequency scattering (SFS) experiments on oil droplets in water (which can be stable for months) offer an alternative way of probing liquid–liquid interfaces.[15,16] The SFS method is a type of nonlinear light scattering[5,17,18] with the added feature that SFS generates spectrally resolved information about all molecules at the interface. As a result, water–vapor and water–oil interfaces can be compared in great detail. In particular, SFS experiments can be used to test the common assumption that water–vapor and water–oil interfaces are structurally similar.

The assumption that the water–vapor and water–oil interfaces are similar is based on their relative permittivities. Water is a medium with a relative permittivity of about 80, while both vapor and oil have lower relative permittivities (∼1 for vapor and roughly <4 for oil). However, the composition of vapor and oil is different, so it is not unreasonable to expect different behavior of sodium dodecyl sulfate (SDS), a prototypical anionic surfactant, at these interfaces. Indeed, early studies of the water–vapor interface[19−23] and of the water–CCl_4 interface[12,24] revealed important differences. Moreover, recent SFS measurements[25,26] on the water–SDS–oil droplet system suggest that (1) the oil molecules are oriented predominantly parallel to the interface and (2) chain defects dominate the SF spectrum of the alkyl tails ($-CH_2-$) of SDS, and (3) the SDS head groups appear to be interacting strongly with the water molecules and (4) the surface coverage does not exceed 0.23 molecule/nm^2.[26] The above findings suggest that there exist important differences between the water–vapor and water–oil interfaces.

Computer simulations allow us to explore these structural differences at a molecular level. Molecular dynamics techniques have been used to probe molecular details of the structural and dynamical properties of SDS at both water–vapor and water–oil interfaces.[27−40] However, these water–SDS/hydrophobic simulations focused on high SDS concentrations (full monolayer), where the water–SDS–oil interface was found to be very similar to that of the water–SDS–vapor interface.[28,40] In contrast, Schweighofer et al. studied the properties of isolated SDS molecules at the water–vapor and water–CCl_4 interfaces.[27,41] However, these simulations provided no information about the organization of SDS at finite interfacial coverages.

Here we report a theoretical, comparative study of the water–vapor and water–decane interfaces with low surface coverage of SDS molecules (1.0 nm^2 per molecule). At these coverages,

Received: May 21, 2012
Revised: July 30, 2012

   dx.doi.org/10.1021/jp304900z | J. Phys. Chem. B XXXX, XXX, XXX–XXX

DS^- ions have considerable conformational freedom and, at the same time, they can interact with each other. Using molecular dynamic simulations, we demonstrate a dramatic difference of SDS behavior at these interfaces. We calculate second-order susceptibilities, which are compared to experimental values.

METHODS

Computation. Molecular dynamics (MD) simulations were performed using the GROMACS program package version 4.0.5.[42] We simulated two different systems: one for the water−vapor interface and a second one for the water−oil interface. The system of water−vapor was composed of 6000 water molecules placed in a prismatic cell of dimensions 4.0 × 4.0 × 30.0 nm yielding a periodically repeated slab of ∼11 nm thickness. After a brief equilibration run of 10 ns, SDS molecules corresponding to the coverage of 1.0 nm^2 per molecule were added above both interfaces and the systems were equilibrated for an additional 10 ns. The water−vapor system was simulated using a constant number of particles (N) and a constant volume (V). The temperature T was kept at 300 K using a velocity-rescaling thermostat of Bussi et al.[43] with a coupling time constant of 1.0 ps. The second system with the water−oil interface was constructed from the water−vapor system, where the free space was filled with 486 decane molecules. The whole system was first heated to 400 K. After 10 ns of equilibration it was cooled to 300 K and equilibrated for another 20 ns. Different copies of the system were obtained using different initial velocities (random seeds). The water−decane systems was kept at constant pressure, temperature, and particle number. The pressure P was fixed at 1 atm (100 kPa) and the temperature T was 300 K.

The temperature was kept constant using the same velocity-rescaling thermostat as above. We allowed the volume to fluctuate in the direction perpendicular to the liquid−liquid interface using the Berendsen's barostat.[44] The time constant of the barostat coupling was set to 2 ps. The time constant of the thermostat coupling constant was 1.0 ps. Production runs were carried out with a 2 fs time step for a total time at least 100 ns. The van der Waals and Coulomb interactions were cutoff at 1.0 nm, and the long-range Coulomb interactions were accounted for using the particle mesh Ewald (PME) method.[45] We employed the recently developed united-atom forcefield for SDS molecules,[46] which is based on the united-atom model for hydrocarbons[47] used for decane. We used the SPC water model,[48] which is compatible with the above force field. Water molecules were kept rigid using the SETTLE algorithm.[49] For the sake of comparison, we also performed tests on system with SPC/E water[48] and system with the TraPPE force field for decane.[50] The electrostatic potential was calculated using Poisson's equation. The charge distribution profile along the normal direction to the interface from simulations was doubly integrated over the normal coordinate.

The intensity of the SFS spectrum, $I_{SFS}(\omega,\theta)$, measured at a scattering angle θ, is related to the effective susceptibility, $\Gamma^{(2)}(\omega,\theta)$, by

$$I_{SFS}(\omega,\theta) \propto \frac{{k_0}^4}{{r_o}^2} I_{IR} I_{VIS} |\Gamma^{(2)}(\omega,\theta)|^2 \tag{1}$$

with

$$\Gamma^{(2)}(\omega,\theta) = \mathrm{Re}|\Gamma^{(2)}| + i\mathrm{Im}|\Gamma^{(2)}| \propto N_s G|F_1(\theta,R); F_2(\theta,R); \chi^{(2)}(\omega)| \tag{2}$$

where k_0 stands for the scattering wave vector, r_o is the distance between the droplet and the detector, and I_{IR} and I_{VIS} are the infrared and visible beam intensities. The effective susceptibility, $\Gamma^{(2)}(\omega,\theta)$, is determined by the droplet radius R and the surface density of vibrational groups N_s. The function G describes the functional dependence of $\Gamma^{(2)}$ on the scattering form factor functions F_1 and F_2, and the second-order surface susceptibility $\chi^{(2)}$ written in eq 3:

$$\begin{pmatrix} \Gamma_1^{(2)} \\ \Gamma_2^{(2)} \\ \Gamma_3^{(2)} \\ \Gamma_4^{(2)} \end{pmatrix} = \begin{pmatrix} 2F_1 - 5F_2 & 0 & 0 & 0 \\ F_2 & 2F_1 & 0 & 0 \\ F_2 & 0 & 2F_1 & 0 \\ F_2 & 0 & 0 & 2F_1 \end{pmatrix} \begin{pmatrix} \chi_1^{(2)} \\ \chi_2^{(2)} \\ \chi_3^{(2)} \\ \chi_4^{(2)} \end{pmatrix} \tag{3}$$

Relative second-order susceptibilities $\chi^{(2)}$ were calculated using eq 4, which relates $\chi^{(2)}$ to the orientation distributions of chemical groups (CH_2, CH_3, SO_3), the tilt angle ϕ (i.e., the angle between the primary axis of the vibration mode and the surface normal), second-order hyperpolarizabilities of the same chemical group $\beta^{(2)}$, and number of the chemical groups N at the interface.

$$\begin{pmatrix} \chi_1^{(2)} \\ \chi_2^{(2)} \\ \chi_3^{(2)} \\ \chi_4^{(2)} \end{pmatrix} = \frac{N\langle\cos(\phi)\rangle}{2} \begin{pmatrix} \frac{5\langle\cos^3(\phi)\rangle - 3\langle\cos(\phi)\rangle}{\langle\cos(\phi)\rangle} & 0 & 0 & 0 \\ \frac{\langle\cos(\phi)\rangle - \langle\cos^3(\phi)\rangle}{\langle\cos(\phi)\rangle} & 2 & 0 & 0 \\ \frac{\langle\cos(\phi)\rangle - \langle\cos^3(\phi)\rangle}{\langle\cos(\phi)\rangle} & 0 & 2 & 0 \\ \frac{\langle\cos(\phi)\rangle - \langle\cos^3(\phi)\rangle}{\langle\cos(\phi)\rangle} & 0 & 0 & 2 \end{pmatrix} \begin{pmatrix} \beta_1 \\ \beta_2 \\ \beta_3 \\ \beta_4 \end{pmatrix} \tag{4}$$

For details on the form factor functions, the relation between the spectral intensities and molecular orientation, see ref 51. In the calculation, we used the parameters of the experiments published in ref 26, which are given in the Results section. The indexes 1−4 of β, $\chi^{(2)}$, and $\Gamma^{(2)}$ refer to a combination of matrix elements, which render eqs 3 and 4 in a simple form (see ref 51 for more details).

RESULTS

Figure 1 shows representative snapshots of the MD simulations with the water/SDS−vapor and water/SDS−decane interfaces. As the figure shows, all four systems are very different. The dodecyl sulfate (DS^-) ions cluster at the water−vapor interface (Figure 1a). The hydrocarbon tails of the DS^- ions are entangled in various orientations. In contrast, no such aggregation is observed at the water−decane interfaces (Figure 1b−d)). We observed two different interfacial structures of "frozen" decane: one with the molecules aligned parallel to the interface and the other with the molecules ordered almost perpendicular to the interface. We will refer to these systems as "decane$_=$" and "decane$_\parallel$", respectively. Both structures appear to coexist in the decane phase in Figure 1b. We studied three replicas of the water/SDS−decane system, leading to the six water−decane interfaces. Both parallel and perpendicular orientations were observed. In contrast, decane modeled with the TraPPE force field[50] behaves radically different: it remains an isotropic liquid up to the interface (Figure 1d)); we denote this system as "decane$_l$".

dx.doi.org/10.1021/jp304900z | J. Phys. Chem. B XXXX, XXX, XXX−XXX

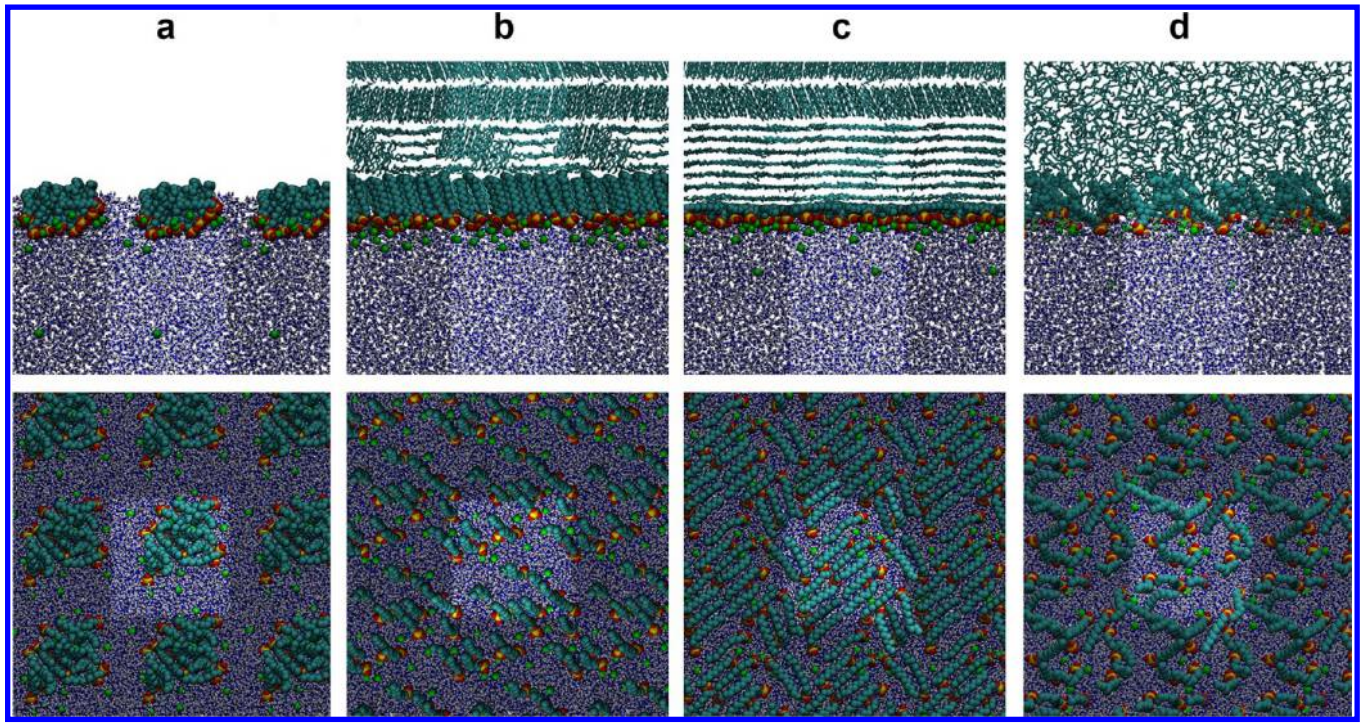

Figure 1. Representative snapshots of (a) the water−SDS/vapor and (b,c,d) the water−SDS/decane systems. There are three conformations of decane: frame b shows "frozen" decane molecules ordered perpendicular with respect to the interface; frame c displays "frozen" decane molecules oriented parallel with respect to the interface; and finally frame d depicts liquid decane. Importantly, SDS aggregates on an air/water interface (a) but not on a water−decane interface (b,c,d). The top row shows a side view, while the bottom row displays a top view of the interface for an SDS coverage of 1 nm^2 per molecule. (Color coding: water oxygen, blue; DS oxygen, red; hydrogen, white; carbon, cyan; sulfur, yellow; and sodium, green.)

Table 1. Calculated Relative Second-Order Susceptibilities for Geometry of Planar Interface Corresponding to SO_3, CH_3, and CH_2 Groups of DS and Their Stretches[a]

	vapor		$decane_{\parallel}$		$decane_{=}$		$decane_{l}$	
SO_3	ss	as	ss	as	ss	as	ss	as
χ_{YYZ}	7.58	3.76	11.50	3.74	11.01	3.83	12.53	3.04
χ_{YZY}	1.26	5.09	1.25	9.01	1.28	8.47	1.02	10.51
χ_{ZYY}	1.26	5.09	1.25	9.01	1.28	8.47	1.02	10.51
χ_{ZZZ}	5.44	7.52	6.72	7.48	6.62	7.65	6.51	6.09
	vapor		$decane_{\parallel}$		$decane_{=}$		$decane_{l}$	
CH_3	ss	as	ss	as	ss	as	ss	as
χ_{YYZ}	6.17	2.86	9.80	4.32	1.42	0.90	7.93	3.07
χ_{YZY}	0.96	4.25	1.45	6.81	0.30	0.83	1.03	5.90
χ_{ZYY}	0.96	4.25	1.45	6.81	0.30	0.83	1.03	5.90
χ_{ZZZ}	4.26	5.72	6.57	8.64	1.17	1.80	5.00	6.15
	vapor		$decane_{\parallel}$		$decane_{=}$		$decane_{l}$	
CH_2	ss		ss		ss		ss	
χ_{YYZ}	2.31		2.86		5.50		0.74	
χ_{YZY}	0.00		0.00		0.00		0.00	
χ_{ZYY}	0.00		0.00		0.00		0.00	
χ_{ZZZ}	2.31		2.86		5.50		0.74	

[a]ss stands for symmetric stretch and as represents antisymmetric stretch. The decane conformation perpendicular to the interfaces is labeled as "||", while the conformation with decane molecules oriented parallel to the interface is labeled as "=". $decane_l$ denotes system with liquid decane.

Calculating the DS^- Signal for SFS. The different molecular conformations in Figure 1 can lead to different SF signals, which can be calculated from our simulations and compared to the experimental values (published in ref 26). The evaluated second-order susceptibilities (relative $\chi^{(2)}$ values) are displayed in Table 1. The employed molecular hyperpolarizabilities are $\beta_1 = 0.0$, $\beta_2 = 1.0$, $\beta_3 = 0.0$, and $\beta_4 = 0.0$ for the symmetric stretch mode (ss) of the CH_2 group. We approximated the hyperpolarizability of the groups with C_{3v} symmetry (CH_3 and SO_3) by $\beta_1 = -0.67$, $\beta_2 = 1.0$, $\beta_3 = 0.0$, and $\beta_4 = 0.0$ for the symmetric stretch mode and $\beta_1 = 2.0$, $\beta_2 = 0.0$, $\beta_3 = 1.0$, and $\beta_4 = 1.0$ for antisymmetric stretch (as) according to ref . We observe that the calculated signal from the SO_3 group is very similar in all the systems, reflecting the same density of DS^- ions. The

dx.doi.org/10.1021/jp304900z | J. Phys. Chem. B XXXX, XXX, XXX−XXX

averaged angle of the SO_3 group, defined as a vector from sulfur to the geometrical center of oxyges, with respect to the surface normal was about 120° at the water−vapor interface and 140° at the water−decane interface. The orientation distribution was not Gaussian, so the mean value should be used with care. In contrast, the relative susceptibility values of the alkyl tails of the DS^- ions differ for the various interfaces that we studied. The largest susceptibility of the CH_3 group was calculated in the decane$_\parallel$ system, 2/3 of this value was obtained for the susceptibility of the water−vapor interface, and one-fifth (1/5) of this value was calculated for the decane$_=$ system. The values for the system with liquid decane are in between the values for water−vapor and decane$_\parallel$. The largest susceptibility values for the CH_2 vibrations of the DS^- ions was obtained for the case that decane is aligned parallel to the interface. For the water−vapor interface and decane$_\parallel$, the value for the CH_2 susceptibility was about a factor 2 smaller. Liquid decane had the smallest susceptibility, about 7 times smaller than the system with decane$_=$.

The effective susceptibilities for scattering experiments $\Gamma^{(2)}$ (Table 2) were evaluated from the second-order susceptibility

Table 2. Calculated Effective Susceptibilities Γ for Scattering Experiments Corresponding to SO_3, CH_3, and CH_2 Groups of DS and Their Stretches[a]

	vapor		decane$_\parallel$		decane$_=$		decane$_\perp$	
SO_3	ss	as	ss	as	ss	as	ss	as
Γ_{SSP}	2.00	1.02	2.87	1.47	2.77	1.42	3.05	1.56
Γ_{SPS}	0.31	1.53	0.44	2.20	0.43	2.13	0.47	2.34
Γ_{PSS}	0.31	1.53	0.44	2.20	0.43	2.13	0.47	2.34
Γ_{PPP}	1.38	2.04	1.98	2.94	1.91	2.83	2.11	3.12
	vapor		decane$_\parallel$		decane$_=$		decane$_\perp$	
CH_3	ss	as	ss	as	ss	as	ss	as
Γ_{SSP}	4.28	2.05	6.71	3.21	1.04	0.50	5.41	1.83
Γ_{SPS}	0.66	3.07	1.04	4.81	0.16	0.75	0.84	3.88
Γ_{PSS}	0.66	3.07	1.04	4.81	0.16	0.75	0.84	3.88
Γ_{PPP}	2.96	4.09	4.64	6.42	0.72	1.00	3.74	5.94
	vapor		decane$_\parallel$		decane$_=$		decane$_\perp$	
CH_2	ss		ss		ss		ss	
Γ_{SSP}	1.54		1.91		3.67		0.51	
Γ_{SPS}	0.00		0.00		0.00		0.00	
Γ_{PSS}	0.00		0.00		0.00		0.00	
Γ_{PPP}	1.54		1.91		3.67		0.51	

[a] ss stands for symmetric stretch and as represents asymmetric stretch. The following experimental setup parameters were employed: average size of scattering particle 100 nm, scattering angle 55°, beam opening angle 15°, and visible beam alignment 12°. Labeling is the same as in Table 1.

$\chi^{(2)}$ values using the parameters from the experimental setup of ref 26 and the relations from ref 51. The average radius of scattering particle 100 nm, scattering angle (θ) 55°, beam opening angle (β) 15°, and visible beam angle (α) 12°. The effective susceptibilities show the same trend as the second-order susceptibilities. In the Discussion we will compare the computed values to the results from the published data.

Water Orientation. We calculated the (normalized) orientational distribution function of water molecules as a function of their distance from the interface (see Figure 2). The interface was defined as the Gibbs dividing surface (GDS), and the water orientation was characterized by the cosine of the water dipole with the surface normal, as shown in Figure 2d. Water molecules located at the GDS were oriented with their dipole pointing

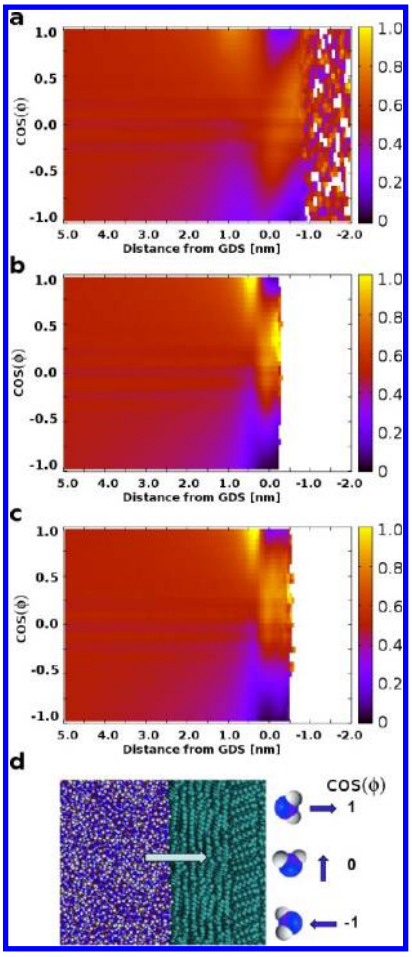

Figure 2. Water dipole orientation distributions with respect to the distance from the interface. Part a depicts the water−vapor interface, while parts b and c display the water−decane interface. Decane molecules are oriented perpendicular to the interface in part b and parallel to the interface in part c. The interface is defined as the Gibbs dividing surface (GDS) of water. Three illustrative orientations of water molecule and its dipole are depicted in part d.

slightly out of the water phase. Water molecules just below the surface (in the direction toward the bulk water) have their dipoles strongly aligned with the surface normal. The orientational distribution function loses structure as the distance from the interface is increased and becomes effectively isotropic at a distance of 3.5 nm from the GDS. The average cos(ϕ) values decay exponentially (approximately). Unsurprisingly, both water−decane interfaces were almost identical in terms of water orientation (Figure 2b,c) but the water−vapor interface is significantly more diffuse than the water−decane interface.

Electrostatic Potential. Figure 3 shows the variation of the electrostatic potential with distance from the interface. Because of the system symmetry, only half of the simulation box is shown. In all three cases, there is a potential minimum at the GDS, where anionic sulfate groups are located. The potential is then screened toward the bulk of the water. The total potential of the water/SDS−decane interface is about −200 mV, while the potential jump at the water/SDS−vapor interface is about twice as large (−400 mV).

DISCUSSION

Our simulations show that the conformations of DS^- at the water−vapor and the water−oil interfaces are very different. The

dx.doi.org/10.1021/jp304900z | J. Phys. Chem. B XXXX, XXX, XXX−XXX

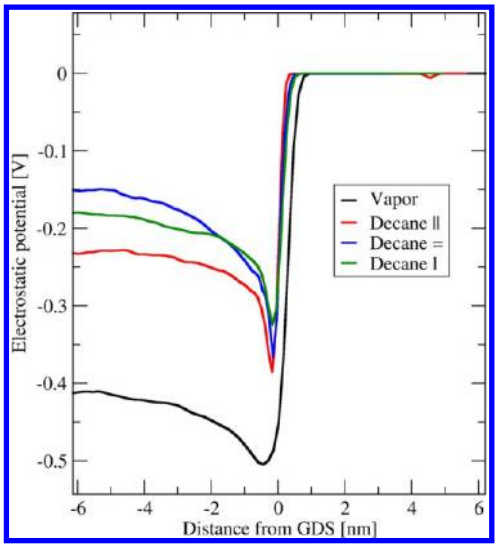

Figure 3. Total electrostatic potentials at the water−SDS/vapor and water−SDS/decane interfaces.

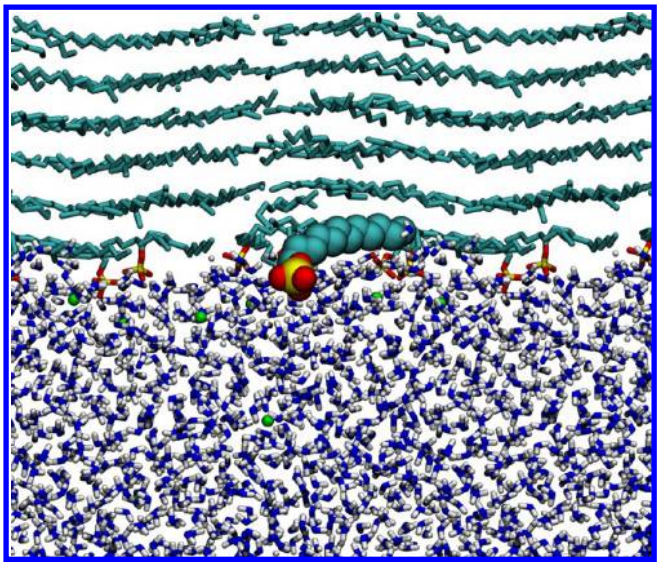

Figure 4. Detailed snapshot of the water−SDS/decane$_=$ interface, where decane molecules are oriented parallel to the interface. One DS molecule was randomly chosen and magnified (shown as spheres). The DS headgroup is inserted in water (oriented almost peprpedicular to the interface), while the hydrocarbon tail is predominantly oriented parallel to the interface. (Color coding as in Figure 1.)

DS^- ions aggregate at the water−vapor interface, while they are homogeneously distributed at the water−decane interface (see Figure 1). The aggregates form due to the dispersion attraction between the DS^- hydrocarbon tails, which overcomes the screened repulsion of the negatively charged DS^- head groups. When the vapor phase is replaced by decane, the net dispersion interaction between the DS^- tails is reduced. This solvent effect removes the driving force for aggregation and the DS^- ions can spread over the water−decane interface. In the case of the water−vapor interface, aggregation is already visible at low coverages, even when only two DS^- ions were present—a situation that corresponds to a coverage of 1 DS^- ions per 8 nm^2.

We find that, irrespective of its orientation, decane at the interface suppresses DS aggregation (see Figure 1). There is a clear problem with the GROMOS force field for decane: under the conditions of our simulations (room temperature), decane should be liquid, yet we find that it freezes in our simulations—the "frozen" layer is as likely to be aligned parallel as perpendicular to the interface. In contrast, simulations based on the TraPPE force field[50] correctly predict that decane is liquid at room temperature.

The easiest way to compare our simulations with the SFS experiments is to compute the ratio of the effective susceptibilities $\Gamma^{(2)}$ of the CH_3 and CH_2 groups at the DS^- ions, which is directly accessible from the experimental data.[12,51] Typically, a ratio value close to zero indicates that the alkyl chains are all well ordered (all-trans conformation), whereas a large nonzero value of the ratio corresponds to a situation where the chains are disordered. The SFS data from SDS (having an odd number of CH_2 groups) were interpreted to display a large degree of chain disorder.[26] The largest ratio was calculated from the decane$_=$ system, where decane and DS^- ions are aligned parallel to the interface and have two gauche defects close to SO_3^- headgroup that is oriented into the water bulk (see Figure 4).

The ratios of the calculated effective susceptibilities from the SFS experiments and our simulations are shown in Table 3. The best agreement with the experiment is for the decane$_=$ system, which is within 10% of the experimental values, e.g., within error of the measurements and force fields. The other simulated systems yield ratios that are off by an order of magnitude including system with liquid decane, where the DS tails have many gauche defects. Note that in all cases the ratio for the SSP polarization combination resulted in lower values than the values for PPP polarization. This trend is in agreement with experiment.[26]

Table 3. Ratio of Relative Effective Susceptibilities of CH_3, CH_2, and SO_3 Groups of the DS Molecule[a]

experiment	hexadecane			
$(CH_2/CH_3)_{SSP}$	3.1			
$(CH_2/CH_3)_{PPP}$	4.7			
$SO_3(ss)_{SSP/PPP}$	1.0			
simulation	vapor	decane$_\|$	decane$_=$	decane$_l$
$(CH_2/CH_3)_{SSP}$	0.36	0.29	3.53	0.10
$(CH_2/CH_3)_{PPP}$	0.50	0.41	5.10	0.14
$SO_3(ss)_{SSP/PPP}$	1.45	1.45	1.45	1.45

[a]Labeling is the same as in Table 1.

It is tempting to explain the results as hexadecane surface freezing with alkyl chains oriented parallel to the interface, since the experimental melting point of hexadecane is at 18° and alkane freezing was observed for the alkane−air interface.[52,53] However, surface freezing was not observed at the neat alkane/water interface.[54] Surfactant-induced surface freezing was observed for hexadecyltrimethylammonium bromide (CTAB).[55] SFG experiments showed drastic changes in the spectra when surface freezing occurred; however, the SFS signal from hexadecane with and without SDS is the same.[25,56] Therefore, it appears that hexadecane molecules are oriented parallel at the interface in a similar way as we see in the decane$_=$ system, yet they remain liquid. The parallel orientation of hexadecane molecules was also put forward in the interpretation of the SFS experiment,[26] in which the chain length of the oil molecules was varied from C6 to C16. The CH_3 signal from the interfacial oil increased for shorter chains. The origin of preference of parallel orientation over the perpendicular orientation for oil molecules is not clear from our simulations. One possible origin could be a preferred interaction of water molecules with CH_2 over CH_3 groups (which is not reflected in the employed united atom force field). This would

dx.doi.org/10.1021/jp304900z | J. Phys. Chem. B XXXX, XXX, XXX−XXX

be in accord with earlier simulations on the water−dodecane interface, where explicit hydrogens and polarizability were included.[40] Other effects such as the motion of droplets might play a role, but are not included in our simulations.

The alignment of the DS molecules parallel to the interface contrasts with its behavior in a full monolayer, where the tails are predominantly perpendicular to the interface and only small differences were found between the water−vapor and the water−CCl_4 interfaces as well as between the water−vapor and water−alkane interfaces.[28,40] The orientation of the SO_3 group of DS^- ion is almost independent of the interface type and of the DS concentration. This finding is consistent with earlier simulation studies of full SDS monolayers.[27,28]

All investigated water interfaces have a similar water orientation distribution. The distribution is broader for the water−vapor interface, which is due to the larger interface fluctuations compared to the water−oil interface. These fluctuations are demonstrated also in density profiles, which show a more diffuse density profile for the water−vapor interface than for the water−decane interface. The average orientation of water molecules at the interface is with the oxygen atoms pointing toward the water similarly to the pure water−vapor interface. This is in agreement with recent SFS measurements.[57] The orientational distribution of the water dipoles at all interfaces is also consistent with previous studies.[27,28,40] Fairly long-range ordering of water molecules is likely to give rise to a strong SFS signal.

The trend of the total electrostatic potential is similar for all interfaces studied and is consistent with potentials found at high SDS coverage at these interfaces, where potentials of 600 mV were calculated.[27,28] In agreement, the shape of the potential profile is mainly determined by water dipole orientation at the interface, negative charged groups of DS, and sodium cations. Indeed, 80% of the sodium ions are found within 1 nm from the GDS. Interestingly, the water−SDS−vapor interface seems to have the least effective screening of the surface charge, which may be caused by the DS aggregation and again demonstrates a difference of the interfaces. A slight deviation among the three water−decane interfaces is within the statistical error. The sharper potential peak at the water−decane interfaces is caused by the smaller width of these interfaces compared to the water−vapor interface.

CONCLUSIONS

The water−vapor interface is often viewed as a model for all water−hydrophobic interfaces. The present study shows that the water−vapor interface is dramatically different from the water−oil interface in terms of the behavior of amphiphilic dodecyl sulfate (DS^-) ions at low concentrations (1 molecule per nm^2). We find that this surfactant aggregates in finite clusters at the water−vapor interface, while it is homogeneously distributed at the water−oil (decane) interface.

We find that the orientation of SDS tails follows the orientation of the alkane molecules. Therefore, it acts as a very good probe of the local alignment of the oil molecules at the water−oil interface. The low coverage results are different from the full monolayers, where the tails are roughly perpendicular to the interface and the overall structure remains similar for the water−vapor and water−oil interfaces.

The employed parametrization of decane molecules based on GROMOS force field "froze" at 300 K, while decane parametrized with TraPPE force field remained liquid. Interestingly, the calculated effective second-order susceptibilities and nonlinear sum frequency scattering intensities of DS^- ions are in quantitative agreement with experimental values only for the system with "frozen" decane, where molecules are oriented parallel to the interface. The values in systems with liquid decane and "frozen" decane with perpendicular orientation to the interface are an order of magnitude lower. This suggests that large alkane molecules (hexadecane) in experiment are oriented parallel to the interface with conformation close to our "frozen" decane molecules. The experiment on the water−decane interface is expected to give rise an order of magnitude lower SFS signal as was calculated in our simulations with liquid decane.

AUTHOR INFORMATION

Corresponding Author

*E-mail: robertvacha@gmail.com.

Notes

The authors declare no competing financial interest.

ACKNOWLEDGMENTS

We are grateful to Daan Frenkel for fruitful comments and discussions. R.V.'s research has been supported by the University of Cambridge (UK), by the European Regional Development Fund (CZ.1.05/1.1.00/02.0068 project CEITEC), and by the EU Seventh Framework Program (Contract No. 286154 SYLICA project). R.V. acknowledges the use of computing facilities of University of Cambridge and MetaCentrum provided under the program "Projects of Large Infrastructure for Research, Development, and Innovations" LM2010005. S.R. thanks the European Research Council (Startup grant no. 240556), the Julia Jacobi Foundation, and the Swiss National Foundation (grant no. 200021_140472).

REFERENCES

(1) Guyot-Sionnest, P.; Hunt, J.; Shen, Y. *Phys. Rev. Lett.* **1987**, *59*, 1597−1600.
(2) Harris, A. L.; Chidsey, C. E. D.; Levinos, N. J.; Loiacono, D. N. *Chem. Phys. Lett.* **1987**, *141*, 350−356.
(3) Bain, C. D. *J. Chem. Soc., Faraday Trans.* **1995**, *91*, 1281.
(4) Vidal, F.; Tadjeddine, A. *Rep. Prog. Phys.* **2005**, *68*, 1095−1127.
(5) Eisenthal, K. B. *Chem. Rev.* **1996**, *96*, 1343−1360.
(6) Richmond, G. L. *Chem. Rev.* **2002**, *102*, 2693−2724.
(7) Shultz, M. J.; Schnitzer, C.; Simonelli, D.; Baldelli, S. *Int. Rev. Phys. Chem.* **2000**, *19*, 123−153.
(8) Richmond, G. *Annu. Rev. Phys. Chem.* **2001**, *52*, 357−89.
(9) Shultz, M. J.; Baldelli, S.; Schnitzer, C.; Simonelli, D. *J. Phys. Chem. B* **2002**, *106*, 5313−5324.
(10) Miranda, P. B.; Shen, Y. R. *J. Phys. Chem. B* **1999**, *103*, 3292−3307.
(11) Feng, R.-r.; Guo, Y.; Lü, R.; Velarde, L.; Wang, H.-f. *J. Phys. Chem. A* **2011**, *115*, 6015−27.
(12) Messmer, M. C.; Conboy, J. C.; Richmond, G. L. *J. Am. Chem. Soc.* **1995**, *117*, 8039−8040.
(13) Scatena, L. F.; Brown, M. G.; Richmond, G. L. *Science (New York, N.Y.)* **2001**, *292*, 908−12.
(14) Wilkinson, K. M.; Qunfang, L.; Bain, C. D. *Soft Matter* **2006**, *2*, 66.
(15) Roke, S.; Roeterdink, W.; Wijnhoven, J.; Petukhov, A.; Kleyn, A. W.; Bonn, M. *Phys. Rev. Lett.* **2003**, *91*, 258302.
(16) Roke, S. *Chemphyschem* **2009**, *10*, 1380−8.
(17) Wang, H.; Yan, E.; Borguet, E.; Eisenthal, K. *Chem. Phys. Lett.* **1996**, *259*, 15−20.
(18) Eisenthal, K. B. *Chem. Rev.* **2006**, *106*, 1462−77.
(19) Ward, R. N.; Duffy, D. C.; Davies, P. B.; Bain, C. D. *J. Phys. Chem.* **1994**, *98*, 8536−8542.
(20) Casson, B. D.; Bain, C. D. *J. Phys. Chem. B* **1998**, *102*, 7434−7441.
(21) Hore, D. K.; Beaman, D. K.; Richmond, G. L. *J. Am. Chem. Soc.* **2005**, *127*, 9356−7.

(22) Johnson, C. M.; Tyrode, E. *Phys. Chem. Chem. Phys.: PCCP* **2005**, *7*, 2635−40.
(23) Harper, K. L.; Allen, H. C. *Langmuir* **2007**, *23*, 8925−31.
(24) Conboy, J. C.; Messmer, M. C.; Richmond, G. L. *Langmuir* **1998**, *14*, 6722−6727.
(25) de Aguiar, H. B.; de Beer, A. G. F.; Strader, M. L.; Roke, S. *J. Am. Chem. Soc.* **2010**, *132*, 2122−3.
(26) de Aguiar, H. B.; Strader, M. L.; de Beer, A. G. F.; Roke, S. *J. Phys. Chem. B* **2011**, *115*, 2970−8.
(27) Schweighofer, K. J.; Essmann, U.; Berkowitz, M. *J. Phys. Chem. B* **1997**, *101*, 10775−10780.
(28) Dominguez, H.; Berkowitz, M. L. *J. Phys. Chem. B* **2000**, *104*, 5302−5308.
(29) Bruce, C. D.; Berkowitz, M. L.; Perera, L.; Forbes, M. D. E. *J. Phys. Chem. B* **2002**, *106*, 3788−3793.
(30) Jang, S. S.; Goddard, W. A. *J. Phys. Chem. B* **2006**, *110*, 7992−8001.
(31) Hantal, G.; Partay, L. B.; Varga, I.; Jedlovszky, P.; Gilányi, T. *J. Phys. Chem. B* **2007**, *111*, 1769−74.
(32) Bresme, F.; Faraudo, J. *Mol. Simul.* **2006**, *32*, 1103−1112.
(33) Bresme, F.; Chacón, E.; Tarazona, P. *Mol. Phys.* **2010**, *108*, 1887−1898.
(34) Bresme, F.; Chacón, E.; Tarazona, P. *Phys. Chem. Chem. Phys.: PCCP* **2008**, *10*, 4704−15.
(35) Bresme, F.; Chacón, E.; Tarazona, P.; Tay, K. *Phys. Rev. Lett.* **2008**, *101*, 1−4.
(36) Bresme, F.; Faraudo, J. *Langmuir* **2004**, *20*, 5127−5137.
(37) Yang, W.; Wu, R.; Kong, B.; Zhang, X.; Yang, X. *J. Phys. Chem. B* **2009**, *113*, 8332−8.
(38) Di Napoli, S.; Gamba, Z. *J. Chem. Phys.* **2010**, *132*, 075101.
(39) Domínguez, H. *J. Phys. Chem. B* **2006**, *110*, 13151−7.
(40) Martinez, H.; Chacon, E.; Tarazona, P.; Bresme, F. *Proc. R. Soc. A: Math., Phys. Eng. Sci.* **2011**, *467*, 1939−1958.
(41) Schweighofer, K. J.; Essmann, U.; Berkowitz, M. *J. Phys. Chem. B* **1997**, *101*, 3793−3799.
(42) Hess, B.; Kutzner, C.; van der Spoel, D.; Lindahl, E. *J. Chem. Theory Comput.* **2008**, *4*, 435−447.
(43) Bussi, G.; Donadio, D.; Parrinello, M. *J. Chem. Phys.* **2007**, *126*, 014101.
(44) Berendsen, H. J. C.; Postma, J. P. M.; van Gunsteren, W. F.; DiNola, A.; Haak, J. R. *J. Chem. Phys.* **1984**, *81*, 3684.
(45) Darden, T.; York, D.; Pedersen, L. *J. Chem. Phys.* **1993**, *98*, 10089.
(46) Sammalkorpi, M.; Karttunen, M.; Haataja, M. *J. Phys. Chem. B* **2007**, *111*, 11722−33.
(47) van Gunsteren, W. F.; Berendsen, H. J. C. *Gromos-87 Manual*; Biomos BV: Nijenborgh 4, 9747 AG Groningen, The Netherlands, 1987.
(48) Berendsen, H. J. C.; Grigera, J. R.; Straatsma, T. P. *J. Phys. Chem.* **1987**, *91*, 6269−6271.
(49) Miyamoto, S.; Kollman, P. A. *J. Comput. Chem.* **1992**, *13*, 952−962.
(50) Martin, M. G.; Siepmann, J. I. *J. Phys. Chem. B* **1998**, *102*, 2569−2577.
(51) de Beer, A. G. F.; Roke, S. *J. Chem. Phys.* **2010**, *132*, 234702.
(52) Wu, X. Z.; Ocko, B. M.; Sirota, E. B.; Sinha, S. K.; Deutsch, M.; Cao, B. H.; Kim, M. W. *Science (New York, N.Y.)* **1993**, *261*, 1018−21.
(53) McKenna, C. E.; Knock, M. M.; Bain, C. D. *Langmuir* **2000**, *16*, 5853−5855.
(54) Tikhonov, A. M.; Mitrinovic, D. M.; Li, M.; Huang, Z.; Schlossman, M. L. *J. Phys. Chem. B* **2000**, *104*, 6336−6339.
(55) Lei, Q.; Bain, C. *Phys. Rev. Lett.* **2004**, *92*, 176103.
(56) Roke, S.; Berg, O.; Buitenhuis, J.; van Blaaderen, A.; Bonn, M. *Proc. Natl. Acad. Sci. U.S.A.* **2006**, *103*, 13310−4.
(57) Vácha, R.; Rick, S. W.; Jungwirth, P.; de Beer, A. G. F.; de Aguiar, H. B.; Samson, J.-S.; Roke, S. *J. Am. Chem. Soc.* **2011**, *133*, 10204−10210.